PHYSICAL REVIEW B **89**, 064428 (2014)

Orbital magnetization of insulating perovskite transition-metal oxides with a net ferromagnetic moment in the ground state

S. A. Nikolaev[1] and I. V. Solovyev[1,2,*]

[1]*Department of Theoretical Physics and Applied Mathematics, Ural Federal University, Mira str. 19, 620002 Ekaterinburg, Russia*

[2]*Computational Materials Science Unit, National Institute for Materials Science, 1-2-1 Sengen, Tsukuba, Ibaraki 305-0047, Japan*

(Received 15 November 2013; published 28 February 2014)

Modern theory of the orbital magnetization is applied to the series of prototype insulating perovskite transition metal oxides (orthorhombic $YTiO_3$, $LaMnO_3$, and YVO_3, as well as monoclinic YVO_3), carrying a net ferromagnetic (FM) moment in the ground state. For these purposes, we use an effective Hubbard-type model, derived from the first-principles electronic structure calculations and describing the behavior of magnetically active states near the Fermi level. The solution of this model in the mean-field Hartree-Fock approximation with the relativistic spin-orbit coupling typically gives us a distribution of the local orbital magnetic moments, which are related to the site-diagonal part of the density matrix $\hat{\mathcal{D}}$ by the "classical" expression $\boldsymbol{\mu}^0 = -\mu_B \mathrm{Tr}\{\hat{\mathbf{L}}\hat{\mathcal{D}}\}$. These moments are usually well quenched by the crystal field. In this work, we evaluate "itinerant" corrections $\Delta\boldsymbol{\mathcal{M}}$ to the net FM moment, suggested by the modern theory. We show that these corrections are small and in most cases can be neglected. Nevertheless, the most interesting aspect of our analysis is that, even for these compounds, which are frequently regarded as prototype Mott insulators, the "itinerant" corrections reveal a strong $\mathbf{k}$ dependence in the reciprocal space, following the behavior of Chern invariants. Therefore, the small value of $\Delta\boldsymbol{\mathcal{M}}$ is the result of strong cancellation of relatively large contributions, coming from different parts of the Brillouin zone. We discuss details as well as possible implications of this cancellation, which depends on the crystal structure as well as the type of the magnetic ground state.

DOI: 10.1103/PhysRevB.89.064428 PACS number(s): 75.30.−m, 75.10.Lp, 71.23.An, 75.50.Dd

I. INTRODUCTION

Orbital magnetism is one of the oldest and most fundamental phenomena. All our present understanding of magnetism developed from the classical concept of orbital motion, which is much older than the concept of spin. The orbital magnetization can be probed by many experimental techniques, including susceptibility measurement, electron paramagnetic resonances, x-ray magnetic circular dichroism, neutron diffraction, etc. [1–4].

At the same time, the orbital magnetism appears to be one of the most difficult and challenging problems for the theory, especially when it comes to the level of first-principles electronic structure calculations. If the methods of spin magnetism are relatively well elaborated today, the study of orbital magnetism is sometimes regarded to be on a primitive stage. There are two reasons for it.

The first one is that the spin magnetism, at least in principle, allows for the description starting from the limit of homogeneous electron gas, which is widely used as an approximation for the exchange-correlation energy (the so-called local spin density approximation or LSDA) in the spin-density functional theory (SDFT). On the contrary, the orbital magnetism always implies some inhomogeneities in the medium, being associated with either the spin-orbit (SO) interaction or the external vector potential, which are necessary to induce the magnetization [5]. Therefore, for the correct description of the orbital magnetization on the level of first-principles electronic structure calculations, it is essential to go beyond the homogeneous electron gas limit. Furthermore, there may be even more fundamental problem, related to the fact that the Kohn-Sham SDFT (even the exact one) does not necessary guarantee to yield correct orbital currents and, therefore, the orbital magnetization, which is defined in terms of these currents [6]. This means that the orbital magnetization (or any related to it quantity) should be treated as an independent variational degree of freedom in the density functional theory (DFT) [7]. Historically, this problem in the calculations of the orbital magnetization was noticed first, and on earlier stages all the efforts were mainly concentrated on the improvement of SDFT, by introducing different kinds of semiempirical orbital functionals (Refs. [8–11]) or moving in the direction of *ab initio* current SDFT (Ref. [12]). Most of these theories emphasized the local character of the orbital magnetization, implying that (i) it can be computed using the standard expression

$$\boldsymbol{\mu}^0 = -\mu_B \mathrm{Tr}\{\hat{\mathbf{L}}\hat{\mathcal{D}}\} \tag{1}$$

for the expectation value of the angular momentum operator $\hat{\mathbf{L}}$ in terms of the site-diagonal part of the density matrix $\hat{\mathcal{D}}$, where $\mu_B = e\hbar/2mc$ is the Bohr magneton, given by the electron charge $(-e)$, its mass (m), the Plank constant $(\hbar)$, and the velocity of light (c); and (ii) the effect of exchange-correlation interactions on $\boldsymbol{\mu}^0$ can be also treated in the local form, by considering only the contributions of some properly screened Coulomb interactions *on the magnetic sites*, coupled to the site-diagonal elements of the density matrix (Ref. [8–10]) or the lattice Green function (Ref. [11]). Even today, the problem of how to "decorate" DFT in order to describe properly the effects of orbital magnetism in solids is largely unresolved and continues to be one of the most important and interesting issues.

Nevertheless, the new turn in the theory of orbital magnetism was not directly related to fundamentals of DFT.

*SOLOVYEV.Igor@nims.go.jp

It was initiated by another fundamental question of how the orbital magnetization should be computed for extended periodic systems. This new direction, which we will refer to as the "modern theory of orbital magnetization," emerged nearly one decade ago and is a logical continuation of the similar theory of electric polarization [13,14]: as the position operator $\mathbf{r}$ is not well defined in the Bloch representation, a similar problem is anticipated for the orbital magnetization operator $(-e/2c)\mathbf{r}\times\mathbf{v}$, which is also expressed through $\mathbf{r}$. Then, the correct consideration of the thermodynamic limit yielded a new and rather nontrivial expression for the orbital magnetization, being another interesting manifestation of the Berry-phase physics [14–19].

The modern theory of the orbital magnetization is basically a one-electron theory. It does not say anything about the form of exchange-correlation interactions. Therefore it would not be right to think that applications of the modern theory will automatically resolve all previous issues, related to the form of the exchange-correlation functional and limitations of LSDA.

Practical implementations of the modern theory of orbital magnetization are still rather limited. Moreover, many of them deal with rather exotic Haldane model Hamiltonian [20], which is typically used in order to illustrate the basic ideas (Refs. [16,17]) and to test computational schemes (Ref. [21]). The first-principles calculations were performed only for ferromagnetic metals Fe, Co, and Ni, where the modern theory slightly improves the values of orbital magnetization in comparison with the experimental data [19,22], and the orbital magnetoelectric coupling in insulators [23].

At the same time, several important aspects of the modern theory remain obscure. To begin with, even if the previous treatment of the orbital magnetization was incomplete, it is not immediately clear what was missing in the "standard" expression (1) and whether it can still be used in practical calculations for real materials. Then, what is the meaning of the new corrections to Eq. (1), suggested by the modern theory?

In this work, we apply the modern theory of the orbital magnetization to the series of representative distorted perovskite transition-metal oxides with the net ferromagnetic (FM) moment in the ground state. Particularly, we consider orthorhombic canted spin ferromagnet $YTiO_3$, and three weak ferromagnets: the orthorhombic $LaMnO_3$ and YVO_3, as well as the monoclinic YVO_3. These compounds differ by the type of the magnetic ground state as well as the microscopic origin of the weak ferromagnetism: regular spin canting away from the collinear A- and G-type antiferromagnetic (AFM) state, caused by Dzyloshinskii-Moriya interactions (Ref. [24]) in the orthorhombic $LaMnO_3$ and YVO_3, respectively [25], versus incomplete compensation of magnetic moments between two crystallographic sublattices in the monoclinic YVO_3 [26]. The magnetic structure of these materials depends on a subtle interplay of the crystal distortion, relativistic SO coupling, and electron correlations in the magnetically active bands. Therefore, from the computational point of view, it is more convenient to work with an effective Hubbard-type model, derived from the first-principles electronic structure calculations, and focusing on the behavior of these magnetically active bands [26]. The previous applications have showed that such a strategy is very promising and the effective model provides a reliable description for the magnetic ground-state properties of $YTiO_3$, YVO_3, and $LaMnO_3$ [26,29,30].

The rest of the paper is organized as follows. In Sec. II, we briefly remind to the reader the main aspects of the modern theory of the orbital magnetization in solids. In Sec. III, we identify the main contributions to the net orbital magnetic moment in the case of basis, when the Bloch wave function is expanded over localized Wannier-type orbitals, centered at the magnetic sites. Then, if the magnetic sites are located in the centers of inversion (the case that we consider), the net orbital magnetic moment will have two contributions: the local one, which is given by the classical expression (1), and an "itinerant" correction to it, suggested by the modern theory. Thus one can trace some analogy with the electric polarization. In the latter case, one can also distinguish a "local" contribution due to static ionic charges, giving rise to classical electric dipoles, and an "anomalous" one, which can be only captured by the Berry phase of the wave functions. Particularly, the behavior of the itinerant moment is closely related to that of Chern invariant, which for the normal insulators can be viewed as a "totally itinerant quantity": the Chern invariant is given by certain Brillion zone (BZ) integral. The individual contributions to this integral in each $\mathbf{k}$ can be finite. However, the total integral, which can be regarded as a local on-site component of some $\mathbf{k}$-dependent property, is identically equal to zero. Then, in Sec. IV, we will briefly explain details of our calculations and in Sec. V, we will present numerical results for $YTiO_3$, YVO_3, and $LaMnO_3$. We will show that the itinerant correction to the net orbital magnetic moment is small. However, this small value is a result of cancellation of relatively large contributions, coming from different parts of the BZ. Finally, in Sec. VI, we will summarize our work.

II. GENERAL THEORY

According to the modern theory of the orbital magnetization [16–18], the net orbital magnetic moment of a normal periodic insulator satisfies the following expression:

$$\mathcal{M}=\frac{e}{2\hbar c}\mathrm{Im}\sum_n\int_{BZ}\frac{d\mathbf{k}}{\Omega}\langle\partial_{\mathbf{k}}u_{n\mathbf{k}}|\times(H_{\mathbf{k}}+E_{n\mathbf{k}})|\partial_{\mathbf{k}}u_{n\mathbf{k}}\rangle, \tag{2}$$

where $u_{n\mathbf{k}}(\mathbf{r})=e^{-i\mathbf{kr}}\psi_{n\mathbf{k}}(\mathbf{r})$ is the cell-periodic eigenstate of the Hamiltonian $H_{\mathbf{k}}=e^{-i\mathbf{kr}}He^{i\mathbf{kr}}$, corresponding to the eigenvalue $E_{n\mathbf{k}}$, the summation runs over occupied states, and the integration goes over the first BZ with the volume Ω. Equation (2) was derived using different theoretical frameworks, including semiclassical dynamics of Bloch electrons [15], the Wannier functions technique [16,17], and the perturbation theory in an external magnetic field [18]. It is important that all these methods yield the same expression for $\mathcal{M}$.

In the modern theory, the behavior of $\mathcal{M}$ is closely related to that of Chern invariants

$$\mathcal{C}=-\frac{1}{2\pi}\mathrm{Im}\sum_n\int_{BZ}d\mathbf{k}\,\langle\partial_{\mathbf{k}}u_{n\mathbf{k}}|\times|\partial_{\mathbf{k}}u_{n\mathbf{k}}\rangle, \tag{3}$$

which was originally introduced to characterize the Hall conductance [27]. For the normal insulators, $\mathcal{C}$ itself vanishes. Nevertheless, the integrand of Eq. (3) (which is also related

to the Berry curvature in the multiband case) can be finite, depending on the symmetry of the crystal and the type of the magnetic ground state. Thus the finite value of $\mathcal{M}$ in normal insulators can be viewed as a result of additional modulation of the Berry curvature by the $\mathbf{k}$-dependent quantities $H_{\mathbf{k}}$ and $E_{n\mathbf{k}}$.

Furthermore, it is understood that all electron-electron interactions are treated in the spirit of Kohn-Sham DFT, that results in the self-consistent determination of the single-particle Hamiltonian H with the SO interaction. It is important that the orbital magnetization (or related to it orbital current) should participate as an independent variable of the energy functional, so that $\mathcal{M}$ can be found through the expectation value of the angular momentum operator in the basis of occupied Kohn-Sham orbitals $\psi_{n\mathbf{k}}(\mathbf{r})$ of the Hamiltonian H [7]. Nevertheless, as was explained in the Introduction, the form of this functional is largely unknown. Therefore, in practical calculations, we have to rely on additional approximations. In the present work, we use H obtained in the mean-field Hartree-Fock (HF) approximation for the effective Hubbard-type model, which was derived from the first-principles electronic structure calculations and is aimed to capture the behavior of the magnetically active states near the Fermi level [26]. The total energy of this HF scheme can be viewed as a functional of the site-diagonal density matrix in the basis of localized Wannier orbitals (which also serve as the basis of the effective model). Thus the basic strategy of the present work is the following. (i) The HF method is expected to reproduce the local part of the orbital moment, which is related to the site-diagonal density matrix by Eq. (1) [10], (ii) We hope that it can also serve as a good starting point for the analysis of other contributions to $\mathcal{M}$. Another possibility is to use current DFT, supplemented with some additional approximations for the exchange-correlation energy [12].

The first term in Eq. (2), which is called the "local circulation" $\mathcal{M}^{LC}$, is the lattice periodic contribution from the bulk Wannier orbitals, while the second term (the "itinerant circulation", $\mathcal{M}^{IC}$) arises from the surface of the sample and remains finite in the thermodynamic limit [16,17]. In the case of normal insulators, both $\mathcal{M}$ and $\mathcal{C}$ can be efficiently computed by replacing $|\partial_{\mathbf{k}} u_{n\mathbf{k}}\rangle$ in Eqs. (2) and (3) by the covariant derivatives:

$$|\tilde{\partial}_{\mathbf{k}} u_{n\mathbf{k}}\rangle = (1 - P_{\mathbf{k}})|\partial_{\mathbf{k}} u_{n\mathbf{k}}\rangle, \tag{4}$$

following the strategy proposed in Ref. [17], where $P_{\mathbf{k}} = \sum_n |u_{n\mathbf{k}}\rangle\langle u_{n\mathbf{k}}|$ is the ground-state projector. The total moment $\mathcal{M} = \mathcal{M}^{LC} + \mathcal{M}^{IC}$ is not affected by the substitution $|\partial_{\mathbf{k}} u_{n\mathbf{k}}\rangle \to |\tilde{\partial}_{\mathbf{k}} u_{n\mathbf{k}}\rangle$. Moreover, the use of covariant derivatives has two major advantages, which allow us to discuss the $\mathbf{k}$ dependence of the net orbital magnetic moments [17]: (i) each contribution, $\mathcal{M}^{LC}$ and $\mathcal{M}^{IC}$, becomes gauge invariant and, therefore, can be measured separately [28], and (ii) not only the BZ integrals, but also the integrands of Eqs. (2) and (3) become gauge invariant in each point of the BZ.

III. ORBITAL MAGNETIZATION AND BASIS

In this section, we will consider how the main expression for $\mathcal{M}$ [Eq. (2)] can be reformulated in the presence of basis. For these purposes, let us expand $|\psi_{n\mathbf{k}}\rangle$ over some basis of localized orbitals $|\phi_\alpha(\mathbf{r} - \mathbf{R})\rangle$, centered at atomic sites $\mathbf{R}$:

$$|\psi_{n\mathbf{k}}\rangle = \frac{1}{\sqrt{N}} \sum_{\alpha\mathbf{R}} c^{\alpha}_{n\mathbf{k}} e^{i\mathbf{k}\mathbf{R}} |\phi_\alpha(\mathbf{r} - \mathbf{R})\rangle, \tag{5}$$

where N is the number of primitive cells, α is a combination of spin and orbital indices (and, if necessary, the site indices in the primitive cell). The basis itself satisfies the orthonormality condition:

$$\langle \phi_{\alpha'}(\mathbf{r} - \mathbf{R}')|\phi_\alpha(\mathbf{r} - \mathbf{R})\rangle = \delta_{\alpha'\alpha}\delta_{\mathbf{R}'\mathbf{R}}. \tag{6}$$

In our case, $\phi_\alpha(\mathbf{r} - \mathbf{R})$ are the Wannier functions, used for the construction of the effective low-energy model [26]. However, "the basis" can be viewed in a more general sense: for example, as the basis of nearly orthogonal linear muffin-tin orbitals of the LMTO method [31], or any orthonormal atomiclike basis.

The use of the basis set is the general practice in numerical calculations. However, apart from the computational issues, the goal of this section is to understand what kind of new contributions is provided by the modern theory [Eq. (2)] in comparison with the standard calculations, which are frequently formulated in the atomiclike basis and use the simplified expression (1) for the orbital magnetization [8–10]. For these purposes, we take the wave functions in the form (5) and substitute them in Eq. (2). Then, the $\mathbf{k}$-space gradient of $|u_{n\mathbf{k}}\rangle$ will have two contributions:

$$\begin{aligned} |\partial_{\mathbf{k}} u_{n\mathbf{k}}\rangle &= -\frac{i}{\sqrt{N}} \sum_{\alpha\mathbf{R}} (\mathbf{r} - \mathbf{R}) e^{-i\mathbf{k}(\mathbf{r}-\mathbf{R})} c^{\alpha}_{n\mathbf{k}} |\phi_\alpha(\mathbf{r} - \mathbf{R})\rangle \\ &\quad + \frac{1}{\sqrt{N}} \sum_{\alpha\mathbf{R}} e^{-i\mathbf{k}(\mathbf{r}-\mathbf{R})} \partial_{\mathbf{k}} c^{\alpha}_{n\mathbf{k}} |\phi_\alpha(\mathbf{r} - \mathbf{R})\rangle \\ &= |\partial_{\mathbf{k}} u_{n\mathbf{k}}\rangle^{\mathrm{I}} + |\partial_{\mathbf{k}} u_{n\mathbf{k}}\rangle^{\mathrm{II}}, \end{aligned} \tag{7}$$

and we have to consider four possible contributions to Eq. (2): $\langle \partial_{\mathbf{k}} u_{n\mathbf{k}}|^{\mathrm{I}} \ldots |\partial_{\mathbf{k}} u_{n\mathbf{k}}\rangle^{\mathrm{I}}$, $\langle \partial_{\mathbf{k}} u_{n\mathbf{k}}|^{\mathrm{I}} \ldots |\partial_{\mathbf{k}} u_{n\mathbf{k}}\rangle^{\mathrm{II}}$, $\langle \partial_{\mathbf{k}} u_{n\mathbf{k}}|^{\mathrm{II}} \ldots |\partial_{\mathbf{k}} u_{n\mathbf{k}}\rangle^{\mathrm{I}}$, and $\langle \partial_{\mathbf{k}} u_{n\mathbf{k}}|^{\mathrm{II}} \ldots |\partial_{\mathbf{k}} u_{n\mathbf{k}}\rangle^{\mathrm{II}}$. Moreover, we assume that all transition-metal sites are located in the inversion centers—the situation, which is indeed realized in the transition-metal perovskites with the $Pbnm$ and $P2_1/a$ structure. Then, the Wannier functions $\{\phi_\alpha(\mathbf{r} - \mathbf{R})\}$ will be either even or odd with respect to this inversion centers, and we will have the following property:

$$\langle \phi_{\alpha'}(\mathbf{r} - \mathbf{R}')|\mathbf{r}|\phi_\alpha(\mathbf{r} - \mathbf{R})\rangle = \mathbf{R}\delta_{\alpha'\alpha}\delta_{\mathbf{R}'\mathbf{R}}. \tag{8}$$

In this case, after some tedious but rather straightforward algebra, which is explained in Ref. [32], one can obtain the following expressions:

$$\begin{aligned} \mathcal{M}^{LC} &= \mathcal{M}^{0} + \Delta\mathcal{M}^{LC} \\ &\equiv -\mu_{\mathrm{B}} \sum_n \sum_{\alpha\alpha'} \int_{BZ} \frac{d\mathbf{k}}{\Omega} c^{\alpha'*}_{n\mathbf{k}} \mathbf{L}^{\alpha'\alpha}_{\mathbf{k}} c^{\alpha}_{n\mathbf{k}} \\ &\quad + \frac{e}{2\hbar c} \mathrm{Im} \sum_n \sum_{\alpha\alpha'} \int_{BZ} \frac{d\mathbf{k}}{\Omega} \partial_{\mathbf{k}} c^{\alpha'*}_{n\mathbf{k}} \times H^{\alpha'\alpha}_{\mathbf{k}} \partial_{\mathbf{k}} c^{\alpha}_{n\mathbf{k}} \end{aligned} \tag{9}$$

and

$$\mathcal{M}^{IC} = \frac{e}{2\hbar c} \mathrm{Im} \sum_n \sum_{\alpha} \int_{BZ} \frac{d\mathbf{k}}{\Omega} E_{n\mathbf{k}}\, \partial_{\mathbf{k}} c^{\alpha*}_{n\mathbf{k}} \times \partial_{\mathbf{k}} c^{\alpha}_{n\mathbf{k}} \tag{10}$$

for the local and itinerant circulation, respectively, where

$$H_{\mathbf{k}}^{\alpha'\alpha} = \frac{1}{N}\sum_{\mathbf{R}\mathbf{R}'} \langle\phi_{\alpha'}(\mathbf{r}-\mathbf{R}')|H|\phi_{\alpha}(\mathbf{r}-\mathbf{R})\rangle\, e^{i\mathbf{k}(\mathbf{R}-\mathbf{R}')} \tag{11}$$

and

$$\mathbf{L}_{\mathbf{k}}^{\alpha'\alpha} = \frac{1}{N}\sum_{\mathbf{R}\mathbf{R}'} \langle\phi_{\alpha'}(\mathbf{r}-\mathbf{R}')|(\mathbf{r}-\mathbf{R}')\times\mathbf{p}|\phi_{\alpha}(\mathbf{r}-\mathbf{R})\rangle e^{i\mathbf{k}(\mathbf{R}-\mathbf{R}')} \tag{12}$$

are the Wannier matrix elements of Hamiltonian and periodic part of the angular momentum operator (divided by $\hbar$), respectively. Moreover, Eq. (12) implies that the momentum operator $\mathbf{p}$ is related to the velocity $\mathbf{v} = (i/\hbar)[H,\mathbf{r}]$ in a "nonrelativistic fashion": $\mathbf{p} = m\mathbf{v}$.

Thus, the local circulation has two terms. The first one ($\boldsymbol{\mathcal{M}}^0$) is the standard contribution, that is given by periodic part of the angular momentum operator in the Wannier basis. Due to orthonormality condition (6), the main contribution to Eq. (12) comes from the site-diagonal elements with $\mathbf{R} = \mathbf{R}'$. It can be best seen in the LMTO formulation [31], where the tail of the basis function $\phi_\alpha(\mathbf{r}-\mathbf{R})$ near the atomic site $\mathbf{R}'$ is expanded over energy derivatives of $\{\phi_\alpha(\mathbf{r}-\mathbf{R}')\}$. Then, since the function is orthogonal to its energy derivative, all contributions with $\mathbf{R} \neq \mathbf{R}'$ in Eq. (12) will vanish after the radial integration. Therefore $\mathbf{L}_{\mathbf{k}}^{\alpha'\alpha}$ does not depend on $\mathbf{k}$ ($\mathbf{L}_{\mathbf{k}}^{\alpha'\alpha} \equiv \mathbf{L}^{\alpha'\alpha}$), and $\boldsymbol{\mathcal{M}}^0$ is given by the standard expression, $\boldsymbol{\mathcal{M}}^0 = -\mu_B \mathrm{Tr}_\alpha\{\hat{\mathbf{L}}\hat{\mathcal{D}}\}$ in terms of the density matrix $\hat{\mathcal{D}} = [\mathcal{D}^{\alpha\alpha'}]$,

$$\mathcal{D}^{\alpha\alpha'} = \sum_n \int_{BZ} \frac{d\mathbf{k}}{\Omega}\, c_{n\mathbf{k}}^{\alpha} c_{n\mathbf{k}}^{\alpha'*},$$

where $\hat{\mathbf{L}} \equiv [\mathbf{L}^{\alpha'\alpha}]$ is the site-diagonal matrix and Tr_α is the trace over α. Thus, the remaining term $\Delta\boldsymbol{\mathcal{M}} = \Delta\boldsymbol{\mathcal{M}}^{LC} + \boldsymbol{\mathcal{M}}^{IC}$ can be viewed as a correction to $\boldsymbol{\mathcal{M}}^0$, suggested by the modern theory. $\Delta\boldsymbol{\mathcal{M}}$ has the same structure as Eq. (2), and can be obtained after replacing $|\partial_{\mathbf{k}} u_{n\mathbf{k}}\rangle$ by the column vector $|\partial_{\mathbf{k}} c_{n\mathbf{k}}\rangle \equiv [\partial_{\mathbf{k}} c_{n\mathbf{k}}^{\alpha}]$ and $H_{\mathbf{k}}$ by the matrix $\hat{H}_{\mathbf{k}} \equiv [H_{\mathbf{k}}^{\alpha'\alpha}]$ in the Wannier basis. The same holds for the Chern invariants (3), where $|\partial_{\mathbf{k}} u_{n\mathbf{k}}\rangle$ should be also replaced by $|\partial_{\mathbf{k}} c_{n\mathbf{k}}\rangle$.

In the following, we will also call $\boldsymbol{\mathcal{M}}^0$ the net *local* magnetic moment and $\Delta\boldsymbol{\mathcal{M}}$ the *itinerant correction* to $\boldsymbol{\mathcal{M}}^0$. This is because, for normal insulators, the Chern invariant itself can be regarded as a totally itinerant quantity. It is proportional to the BZ integral of the Berry curvature. The Berry curvature itself is $\mathbf{k}$-dependent. However, the local component of it, that is given by the BZ integration, is identically equal to zero. Therefore it is logical to view $\Delta\boldsymbol{\mathcal{M}}$, whose form is similar to $\boldsymbol{\mathcal{C}}$, also as an itinerant contribution to the net orbital magnetic moment. Moreover, for the fully localized states, $\hat{H}_{\mathbf{k}}$ and $E_{n\mathbf{k}}$ will not depend on $\mathbf{k}$. Therefore, in this case, $\Delta\boldsymbol{\mathcal{M}}$ will vanish, similar to $\boldsymbol{\mathcal{C}}$. This is another reason why $\Delta\boldsymbol{\mathcal{M}}$ can be associated with the itinerant contribution to the orbital magnetic moment. One can also paraphrase this discussion in the following way: the Berry curvature in the BZ integrals (9) and (10) acts as a "filter," which separates the local part of the orbital magnetization from the itinerant one.

IV. TECHNICAL DETAILS

All numerical calculations, reported in this work, have been performed for the effective low-energy Hubbard-type model, derived from the first-principles electronic structure calculations. Such a model is regarded as a bridge between first-principles electronic structure calculations and the model Hamiltonian approach. Moreover, the model allows us to treat the problem of electron correlations beyond conventional approximations employed in the first-principles calculations. Below, we will outline the main ideas of this approach. All details, including the behavior of model parameters, can be found in the review paper (Ref. [26]) and in previous publications (Refs. [29,30]).

The multiorbital Hubbard Hamiltonian,

$$\hat{H} = \sum_{\mathbf{R}\mathbf{R}'}\sum_{\alpha\alpha'} t_{\mathbf{R}\mathbf{R}'}^{\alpha\alpha'} \hat{c}_{\mathbf{R}\alpha}^{\dagger}\hat{c}_{\mathbf{R}'\alpha'} + \frac{1}{2}\sum_{\mathbf{R}}\sum_{\{\alpha\}} U_{\alpha\alpha'\alpha''\alpha'''}^{\mathbf{R}} \hat{c}_{\mathbf{R}\alpha}^{\dagger}\hat{c}_{\mathbf{R}\alpha''}^{\dagger}\hat{c}_{\mathbf{R}\alpha'}\hat{c}_{\mathbf{R}\alpha'''}, \tag{13}$$

is constructed in the basis of Wannier functions $\{\phi_\alpha(\mathbf{r}-\mathbf{R})\}$ for the magnetically active bands near the Fermi level, starting from the local-density approximation (LDA). For the considered compounds, these are the t_{2g} bands in the case of $YTiO_3$ and YVO_3, and all $3d$ bands in the case of $LaMnO_3$.

The first step is the construction of complete basis of Wannier orbitals for these low-energy bands. In our case, the Wannier function were generated using the projector-operator method (Refs. [26,33,34]) and orthonormal basis orbitals of the LMTO method (Ref. [31]) as the trial wave functions. As the LMTO basis functions are already well localized, typically such procedure allows us to generate well localized Wannier functions. Then, the one-electron part of the model is identified with the matrix elements of LDA Hamiltonian (H_{LDA}) in the Wannier basis: $t_{\mathbf{R}\mathbf{R}'}^{\alpha\alpha'} = \langle\phi_\alpha(\mathbf{r}-\mathbf{R})|H_{\mathrm{LDA}}|\phi_{\alpha'}(\mathbf{r}-\mathbf{R}')\rangle$. Since the Wannier basis is complete in the low-energy part of the spectrum, the construction is exact in a sense that the band structure, obtained from $t_{\mathbf{R}\mathbf{R}'}^{\alpha\alpha'}$, coincides with the one of LDA.

Matrix elements of screened Coulomb interactions at some atomic site $\mathbf{R}$ can be also calculated in the Wannier basis, by employing the constrained random-phase approximation (RPA) technique [35]. Since the constrained RPA technique is very time consuming (and still not affordable for considered low-symmetry compounds, containing 20 atoms in the primitive cell), we apply additional approximations, which were discussed in Ref. [26]. Namely, first we evaluate the screened Coulomb and exchange interactions between atomic $3d$ orbitals, using fast and more suitable for these purposes constrained LDA technique. This step includes the screening by outer (non-$3d$) electrons and due to the relaxation of the atomic $3d$ wave functions. After that, we consider additional channel of screening caused by the $3d \rightarrow 3d$ transitions in the polarization function (the so-called "self-screening"), involving these atomic basis orbitals, in the framework of constrained RPA technique. The so-obtained parameters of Coulomb interactions are in good agreement with results of full-scale constrained RPA calculations [36].

After the construction, the model was solved using unrestricted HF approach. The main point here is that the static

lattice distortion lifts the orbital degeneracy and substantially suppress the quantum fluctuations in all considered compounds. Thus, the ground state of these systems can be described reasonably well by a single Slater determinant, that justifies the use of the HF approach. For instance, using model parameters, derived from the first-principles calculations, and solving the obtained model in the HF approximation, one can successfully reproduce the experimental FM, A-type AFM, G-type AFM, and C-type AFM ground state in $YTiO_3$, $LaTiO_3$, orthorhombic YVO_3, and monoclinic YVO_3, respectively. If necessary, the HF approximation can be additionally improved by considering the regular perturbation theory expansion for electron correlations near the magnetic ground state. The validity of this strategy was demonstrated in Refs. [26,29,30].

The HF approximation for the low-energy model, derived from the first-principles calculations, has many similarities with the LDA+U approach [10,37]. As was demonstrated in Ref. [29], both techniques provide very similar description for the considered distorted perovskite oxides. The main difference is that the model is formulated in the restricted basis of states close to the Fermi level, while LDA+U is formally an "all-electron" approach. However, the latter advantage of LDA+U is typically eliminated by additional (and, sometimes, rather artificial) approximations for the double-counting terms and the division of all states into "localized" and "delocalized" ones. Another good point of the effective Hamiltonian approach is that it can be relatively easy used for the analysis of complex noncollinear magnetic structures, resulting from the competition of many magnetic interactions in the system, that is very important for understanding the origin of multiferroic effect [38–40].

Finally, we discuss some specific points, related to calculations of the orbital magnetization. Strictly speaking, if the model Hamiltonian H includes the SO interaction term,

$$H_{\mathrm{SO}} = \frac{\hbar}{4m^2c^2}\boldsymbol{\sigma} \times \boldsymbol{\nabla} V \cdot \mathbf{p}, \tag{14}$$

which originates from Pauli equations and is valid in the second order of $1/c$, the velocity operator $\mathbf{v} = (i/\hbar)[H, \boldsymbol{r}]$ will consists of two contributions:

$$\mathbf{v} = \frac{\mathbf{p}}{m} + \frac{\hbar}{4m^2c^2}\boldsymbol{\sigma} \times \boldsymbol{\nabla} V. \tag{15}$$

The theory of orbital magnetization implies that the second term in Eq. (15) can be neglected, that results in the nonrelativistic expression $\mathbf{p} = m\mathbf{v}$. This can be done because the contribution of the second term of Eq. (15) to the orbital magnetic moment (2) is of the order of $1/c^3$, which is formally beyond the accuracy of Pauli equations.

In order to calculate $\tilde{\partial}_{\mathbf{k}} c_{n\mathbf{k}}$ along the direction i of the BZ, we have used the discretized covariant derivative technique, which is well suited for insulators [17,19]:

$$\tilde{\partial}_i c_{n\mathbf{k}} = \frac{1}{2|\mathbf{q}|}(\tilde{c}_{n\mathbf{k}+\mathbf{q}} - \tilde{c}_{n\mathbf{k}-\mathbf{q}}), \tag{16}$$

where $\mathbf{q}$ is the vector that connects $\mathbf{k}$ with the nearby point in the direction i and $\tilde{c}_{n\mathbf{k}+\mathbf{q}}$ is the "dual" state, defined in terms of the overlap matrix $(S_{\mathbf{k},\mathbf{k}+\mathbf{q}})_{nn'} = \langle c_{n\mathbf{k}} | c_{n'\mathbf{k}+\mathbf{q}} \rangle$ as

$$\tilde{c}_{n\mathbf{k}+\mathbf{q}} = \sum_{n'} \left(S^{-1}_{\mathbf{k},\mathbf{k}+\mathbf{q}}\right)_{n'n} c_{n'\mathbf{k}}. \tag{17}$$

As for the $\mathbf{k}$-space integration, we have used the grid of about $70\times70\times50$ points in the first BZ, which guarantees an excellent convergence for $\Delta\boldsymbol{\mathcal{M}}$ depending on the number of $\mathbf{k}$ points [32].

V. RESULTS

A. $YTiO_3$

$YTiO_3$ crystallizes in the orthorhombic $Pbnm$ structure (in our calculations, we used the experimental structure parameters, measured at 2 K) [41]. Below $T_C \approx 29$ K, it forms the canted FM structure, where the net FM moment is parallel to the orthorhombic $\boldsymbol{c}$ axis. Two other components of the magnetic moments, parallel to the orthorhombic $\boldsymbol{a}$ and $\boldsymbol{b}$ axes, are ordered antiferromagnetically. The type of this ordering is G and A, respectively. Such magnetic structure can be abbreviated as $G_{\boldsymbol{a}}$-$A_{\boldsymbol{b}}$-$F_{\boldsymbol{c}}$. It was successfully reproduced by our mean-field HF calculations for the low-energy model. The details of these calculations can be found in Ref. [29] and the obtained magnetic structure is summarized in Fig. 1. In this case, the vector of the spin magnetic moment at the site 1 is $(-0.021, -0.127, 0.986)$ μ_{B} and the vector $\boldsymbol{\mu}^0$ of orbital magnetic moment is $(-0.033, -0.001, -0.018)$ μ_{B}. Therefore the net local orbital magnetic moment $\mathcal{M}^0_c$ (per one primitive cell of $YTiO_3$, containing four Ti atoms) is -0.072 μ_{B} (Table I). As was explained above, it is parallel to the $\boldsymbol{c}$ axis.

Then, we evaluate the itinerant correction $\Delta\boldsymbol{\mathcal{M}}$, resulting from the local and itinerant circulation terms. These results are summarized in Table I. Because of the symmetry, the projections of $\Delta\boldsymbol{\mathcal{M}}$ onto the orthorhombic $\boldsymbol{a}$ and $\boldsymbol{b}$ axes are identically equal to zero [42]. The $\boldsymbol{c}$ projection ($\Delta\mathcal{M}_c$) is finite. However, it is more than two orders of magnitude smaller than $\mathcal{M}^0_c$ and, therefore, can be safely neglected. In principle, this result is anticipated for the considered transition-metal oxides, which are frequently regarded as Mott insulators and in which the magnetically active $3d$ states are relatively well localized.

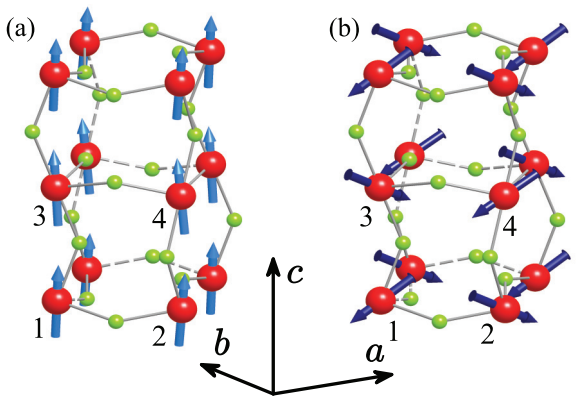

FIG. 1. (Color online) Distribution of spin (a) and orbital (b) magnetic moments as obtained in the mean-field Hartree-Fock calculations for the low-energy model of $YTiO_3$ [29]. The titanium atoms are indicated by the big red (dark) spheres and the oxygen atoms are indicated by the small green (grey) spheres. For the sake of clarity, the arrows for the orbital magnetic moments were scaled in order to have the same length as for the spin magnetic moments.

TABLE I. Different contributions to the net orbital magnetic moment, as obtained in the mean-field Hartree-Fock calculations for the low-energy model: the local moment $\mathcal{M}^0$, given by periodic part of the orbital momentum operator in the Wannier basis, and two itinerant contributions, due to the local and itinerant circulation ($\Delta\mathcal{M}^{LC}$ and $\mathcal{M}^{IC}$, respectively). All values are in μ_B per one primitive cell, containing four transition-metal sites.

Compound	Direction	$\mathcal{M}^0$	$\Delta\mathcal{M}^{LC}$	$\mathcal{M}^{IC}$	$\Delta\mathcal{M}^{LC}+\mathcal{M}^{IC}$
$YTiO_3$ ($Pbnm$)	$\|\|c$	−0.072	-1.22×10^{-5}	2.63×10^{-4}	2.50×10^{-4}
$LaMnO_3$ ($Pbnm$)	$\|\|c$	−0.032	1.05×10^{-4}	-2.28×10^{-4}	-1.23×10^{-4}
YVO_3 ($Pbnm$)	$\|\|a$	−0.004	-6.75×10^{-4}	-1.30×10^{-4}	-8.05×10^{-4}
YVO_3 ($P2_1/a$)	$\|\|b$	−0.020	3.30×10^{-6}	-2.29×10^{-5}	-1.96×10^{-5}

Nevertheless, it is interesting to gain some insight by investigating the origin of such a small value. For these purposes, we analyze the integrand

$$\Delta\mathcal{M}(\mathbf{k}) = \frac{e}{2\hbar c}\,\mathrm{Im}\sum_n \langle\partial_{\mathbf{k}}c_{n\mathbf{k}}|\times(\hat{H}_{\mathbf{k}}+E_{n\mathbf{k}})|\partial_{\mathbf{k}}c_{n\mathbf{k}}\rangle$$

of

$$\Delta\mathcal{M} = \int_{BZ}\frac{d\mathbf{k}}{\Omega}\,\Delta\mathcal{M}(\mathbf{k})$$

and plot it along high-symmetry directions of the BZ (see Fig. 2). Notations of the high-symmetry points of the BZ were taken from the book of Bradley and Cracknell [43]. We obtained that two components, $\Delta\mathcal{M}_a(\mathbf{k})$ and $\Delta\mathcal{M}_b(\mathbf{k})$, are identically equal to zero in each $\mathbf{k}$ point, while $\Delta\mathcal{M}_c(\mathbf{k})$ can be finite and, moreover, strongly depend on $\mathbf{k}$. This behavior is consistent with the G_a-A_b-F_c symmetry of the magnetic ground state [42]. $\Delta\mathcal{M}_c(\mathbf{k})$ reaches its maximal value of 0.088 μ_B in the point $Y=(0,\frac{1}{2},0)$ of the BZ (in units of reciprocal lattice translations), which is comparable with $\mathcal{M}_c^0$. Thus the individual contributions $\Delta\mathcal{M}_c(\mathbf{k})$ can be large. However, there is also a large cancelation between positive and negative contributions to $\Delta\mathcal{M}_c$ around the Y and $X=(\frac{1}{2},0,0)$ points, respectively. Similar situation occurs at the BZ boundary $k_c=\frac{1}{2}$, where again the large positive contribution around $T=(0,\frac{1}{2},\frac{1}{2})$ is nearly canceled by the negative contribution around $U=(\frac{1}{2},0,\frac{1}{2})$. This result is summarized in Fig. 3, where we plot $\Delta\mathcal{M}_c(k_a,k_b,k_c)$ for $k_c=0$ and $\frac{1}{2}$, as well as its planar average over k_a and k_b:

$$\Delta\mathcal{M}_c(k_c) = \frac{|\boldsymbol{a}||\boldsymbol{b}|}{4\pi^2}\int_{-\pi/a}^{\pi/a}dk_a\int_{-\pi/b}^{\pi/b}dk_b\,\Delta\mathcal{M}_c(k_a,k_b,k_c).$$

One can clearly see that $\Delta\mathcal{M}_c(k_a,k_b,k_c)$ only weakly depends on k_c. For each k_c, there is a strong cancellation of the positive and negative contributions to $\Delta\mathcal{M}_c(k_a,k_b,k_c)$, arising from $\mathbf{k}=(0,\frac{1}{2},k_c)$ and $(\frac{1}{2},0,k_c)$, respectively. This cancellation readily explains the small value of $\Delta\mathcal{M}_c(k_c)$. Finally, the integration of $\Delta\mathcal{M}_c(k_c)$ over k_c yields the total value of $\Delta\mathcal{M}_c$, reported in Table I. Thus the small value of $\Delta\mathcal{M}_c$ is the result of strong cancellation of relatively large contributions $\Delta\mathcal{M}_c(\mathbf{k})$, coming from different parts of the BZ. Moreover, the strong $\mathbf{k}$-dependence of $\Delta\mathcal{M}$ implies that, after the Fourier transformation to the real space, in addition to the small site-diagonal component, this quantity will have a large nonlocal (or off-diagonal with respect to the atomic sites) part. Since the $\mathbf{k}$ dependence is smooth, this Fourier series should converge, that justifies the use of the real-space analysis.

In the rest of this section, we will show that the cancellation of different contributions to $\Delta\mathcal{M}$ in the reciprocal space is a generic result, which can be expected for other Mott insulators,

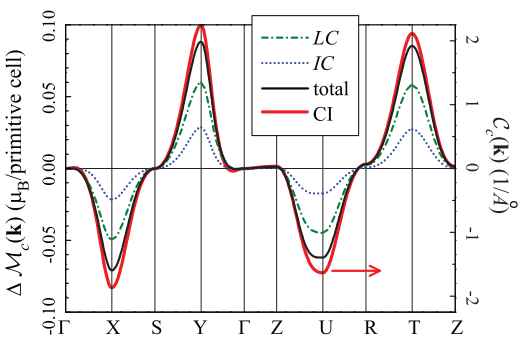

FIG. 2. (Color online) Behavior of itinerant contributions to the net orbital magnetic moment in $YTiO_3$ (left axis) and corresponding Chern invariant (CI, right axis) in the reciprocal space, along high-symmetry directions of the Brillouin zone. Two partial contributions to the net orbital moment, associated with the local ($\Delta\mathcal{M}^{LC}$) and itinerant ($\mathcal{M}^{IC}$) circulation, are denoted as LC and IC, respectively, and the sum of these two contributions is denoted as "total".

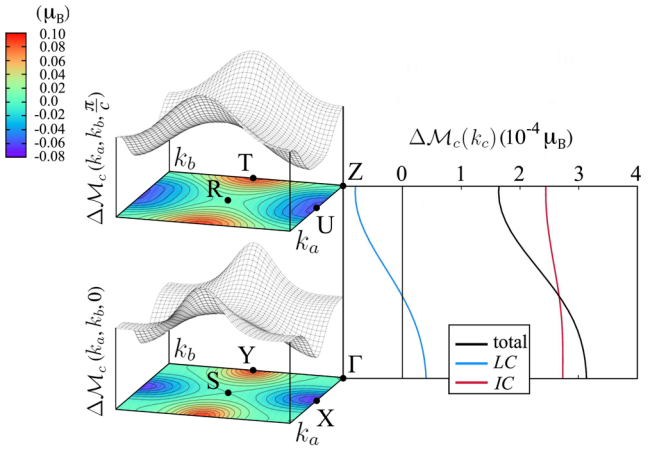

FIG. 3. (Color online) (Left) Three-dimensional plot of $\Delta\mathcal{M}_c(\mathbf{k})\equiv\Delta\mathcal{M}_c(k_a,k_b,k_c)$ for $k_c=0$ and $\frac{1}{2}$ in the case of $YTiO_3$. (Right) The k_c dependence of $\Delta\mathcal{M}_c(k_c)$, obtained after the integration of $\Delta\mathcal{M}_c(\mathbf{k})$ over k_a and k_b, and its partial contributions associated with local and itinerant circulation terms (LC and IC, respectively).

carrying a net FM moment in the ground state. The intuitive reason is the following. As was already pointed out in Sec. II, the behavior of $\Delta\boldsymbol{\mathcal{M}}$ is closely related to that of the Chern invariants. For our purposes, it is convenient to rewrite $\boldsymbol{\mathcal{C}}$ in the following form:

$$\boldsymbol{\mathcal{C}} = \frac{1}{\Omega}\int_{BZ} d\mathbf{k}\,\boldsymbol{\mathcal{C}}(\mathbf{k}),$$

where

$$\boldsymbol{\mathcal{C}}(\mathbf{k}) = -\frac{\Omega}{2\pi}\mathrm{Im}\sum_n \langle\partial_{\mathbf{k}} c_{n\mathbf{k}}| \times |\partial_{\mathbf{k}} c_{n\mathbf{k}}\rangle.$$

For the normal insulators, $\boldsymbol{\mathcal{C}}$ is zero, and this property is perfectly reproduced by our calculations. However, due to the specific symmetry of the $G_{\boldsymbol{a}}$-$A_{\boldsymbol{b}}$-$F_{\boldsymbol{c}}$ ground state of $YTiO_3$ [42], the integrand $\mathcal{C}_c(\mathbf{k})$ can be finite in the individual $\mathbf{k}$ points, while two other projections of $\boldsymbol{\mathcal{C}}(\mathbf{k})$ onto the orthorhombic $\boldsymbol{a}$ and $\boldsymbol{b}$ axes are identically equal to zero. Furthermore, the $\mathbf{k}$ dependence of $\mathcal{C}_c(\mathbf{k})$ is very close to that of $\Delta\mathcal{M}_c(\mathbf{k})$ (see Fig. 2). Thus, in the case of Chern invariant $\mathcal{C}_c(\mathbf{k})$, the contributions from different parts of the BZ exactly cancel each other. However, in the expression for $\Delta\mathcal{M}_c$, the $\mathbf{k}$ dependence of $\mathcal{C}_c(\mathbf{k})$ for each band is additionally modulated with $\mathbf{k}$-dependent $\hat{H}_{\mathbf{k}}$ and $E_{n\mathbf{k}}$, that leads to a small but finite value of $\Delta\mathcal{M}_c$ (see Table I). It also explains why $\Delta\mathcal{M}_c^{LC}(\mathbf{k})$ and $\mathcal{M}_c^{IC}(\mathbf{k})$ reveal very similar $\mathbf{k}$ dependence: in both cases, it is dictated by the $\mathbf{k}$ dependence of $\mathcal{C}_c(\mathbf{k})$, which appears to be more fundamental quantity. Below, we will show that similar properties hold for other compounds, exhibiting different types of the lattice distortion and, therefore, the magnetic ground state.

B. $LaMnO_3$

$LaMnO_3$ is another compound, crystallizing in the orthorhombic $Pbnm$ structure [44]. It has the same $G_{\boldsymbol{a}}$-$A_{\boldsymbol{b}}$-$F_{\boldsymbol{c}}$ type of the magnetic ground state, which is realized below $T_N \approx 140$ K [45]. This magnetic ground state was successfully reproduced in our mean-field HF calculations for the low-energy model. The basic difference from $YTiO_3$ is that the spin magnetic structure is nearly A-type AFM and the FM canting of spins in the $\boldsymbol{c}$ direction is really small. In this sense, $LaMnO_3$ can be viewed as a canonical weak ferromagnet. Nevertheless, the orbital magnetic structure is strongly deformed: in comparison with the spin one, there is a large deviation from the collinear A-type AFM alignment and an appreciable canting of the orbital magnetic moments in the $\boldsymbol{a}$ and $\boldsymbol{c}$ directions, which can be seen even visually in Fig. 4.

The vector of spin magnetic moment at the site 1 is $(0.354, 3.952, 0.111)\ \mu_B$ and the one of orbital magnetic moment $\boldsymbol{\mu}^0$ is $(-0.030, -0.057, -0.008)\ \mu_B$. Thus the net orbital magnetic moment $\boldsymbol{\mathcal{M}}^0$ is $-0.032\ \mu_B$ (Table I).

The behavior of $\Delta\boldsymbol{\mathcal{M}}(\mathbf{k})$ is qualitatively the same as in $YTiO_3$: it has similar structure and similar type of cancellation between different parts of the BZ (see Fig. 5). Taking into account that $YTiO_3$ and $LaMnO_3$ have the same type of the orthorhombic structure and the magnetic ground state, such similarity is not surprising. The main difference is in the magnitude of the effect, which is much more pronounced in $LaMnO_3$: the values of $\Delta\mathcal{M}_c(\mathbf{k})$ in the Y and T points are

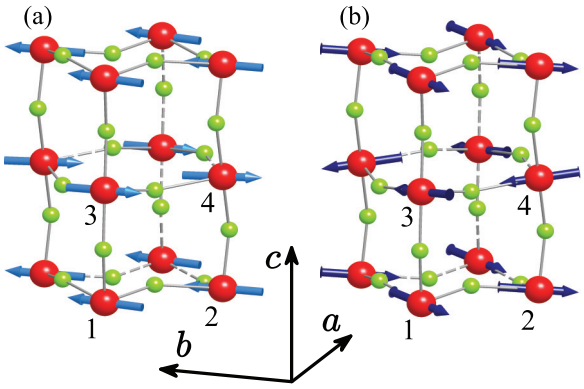

FIG. 4. (Color online) Distribution of spin (a) and orbital (b) magnetic moments as obtained in the mean-field Hartree-Fock calculations for the low-energy model of $LaMnO_3$. The manganese atoms are indicated by the big red (dark) spheres and the oxygen atoms are indicated by the small green (grey) spheres. For the sake of clarity, the arrows for the orbital magnetic moments were scaled in order to have the same length as for the spin magnetic moments.

0.154 μ_B and 0.159 μ_B, respectively, which exceed $\mathcal{M}_c^0$ by factor five. However, there is again a strong cancellation with the negative contributions around the X and U points of the BZ, which, after the integration, leads to the small value of $\Delta\mathcal{M}_c$. Moreover, in $LaMnO_3$ there is an appreciable cancellation between *LC* and *IC* contributions to $\Delta\mathcal{M}_c$ (see Table I).

Like in $YTiO_3$, the $\mathbf{k}$ dependence of $\Delta\mathcal{M}_c(\mathbf{k})$ in $LaMnO_3$ follows the form of $\mathcal{C}_c(\mathbf{k})$ (Fig. 5). Nevertheless, one interesting aspect is that the amplitude of $\mathcal{C}_c(\mathbf{k})$ in $LaMnO_3$ is smaller than in $YTiO_3$ (see Fig. 2), while for $\Delta\mathcal{M}_c(\mathbf{k})$ the situation is exactly the opposite. This difference may be related to the number of occupied bands (16 in the case of $LaMnO_3$ versus 4 in the case of $YTiO_3$). Thus, the amplitude of $\Delta\mathcal{M}_c(\mathbf{k})$ may be larger in $LaMnO_3$ because the number of occupied bands is larger. Moreover, $YTiO_3$ is a t_{2g} system, while the net orbital moment in $LaMnO_3$ contains a contribution of much less localized e_g

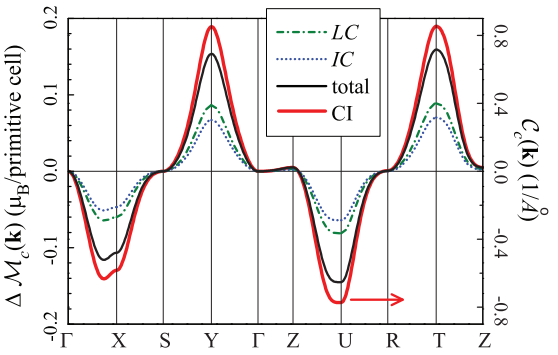

FIG. 5. (Color online) Behavior of itinerant contributions to the net orbital magnetic moment in $LaMnO_3$ (left axis) and corresponding Chern invariant (CI, right axis) in the reciprocal space, along high-symmetry directions of the Brillouin zone. Two partial contributions to the net orbital moment, associated with the local ($\Delta\boldsymbol{\mathcal{M}}^{LC}$) and itinerant ($\boldsymbol{\mathcal{M}}^{IC}$) circulation, are denoted as *LC* and *IC*, respectively, and the sum of these two contributions is denoted as "total".

electrons. Therefore it is reasonable to expect that the itinerant moment $\Delta\mathcal{M}_c(\mathbf{k})$ will be larger in $LaMnO_3$.

C. YVO_3

YVO_3 has two crystallographic modifications: orthorhombic $Pbnm$, which is realized below 77 K, and monoclinic $P2_1/a$ above 77 K (in our calculations, we use the experimental structure parameters at 65 and 100 K, respectively) [46].

The magnetic structure, realized in the orthorhombic $Pbnm$ phase is F_a-C_b-G_c (see Fig. 6). According to the mean-field HF calculations for the low-energy model, the vector of spin magnetic moment at the site 1 is $(-0.016, 0, 1.969)\ \mu_B$ and the vector of orbital magnetic moment is $(-0.001, 0.001, -0.186)\ \mu_B$. Thus, the $\boldsymbol{c}$ projection clearly dominates, while two other projections are substantially smaller. The net orbital magnetic moment $\mathcal{M}_a^0$ is only $-0.004\ \mu_B$, which is parallel to the orthorhombic $\boldsymbol{a}$ axis.

The monoclinic phase of YVO_3 has two inequivalent pairs of V sites, which are denoted in Fig. 6 as (1,2) and (3,4). Within each pair, the $\boldsymbol{a}$ and $\boldsymbol{c}$ projections of the magnetic moments are coupled antiferromagnetically, while the $\boldsymbol{b}$ projections are ferromagnetic. According to the mean-field HF calculations for the low-energy model, the vectors of spin magnetic moments at the sites 1 and 3 are $(-0.850, 0.077, 1.785)\ \mu_B$ and $(-0.875, -0.032, 1.764)\ \mu_B$, respectively, and the vectors of orbital magnetic moments are $(0.074, -0.046, -0.173)\ \mu_B$ and $(0.043, 0.036, -0.073)\ \mu_B$, respectively. The local orbital magnetic moments in the sublattice (3,4) are substantially smaller due to additional quenching by stronger crystal field (see Ref. [29] for details). Thus there is a partial cancellation of the FM magnetization between two sublattices. However, due to the additional quenching in the sublattice (3,4), this cancellation is not complete and the system remains weakly ferromagnetic. The net orbital magnetic moment $\mathcal{M}_b^0$ is $-0.02\ \mu_B$, which is parallel to the monoclinic $\boldsymbol{b}$ axis. The directions of the net magnetic moment and, therefore, the type of the magnetic ground state in the orthorhombic and monoclinic phases are well consistent with the experimental data [47].

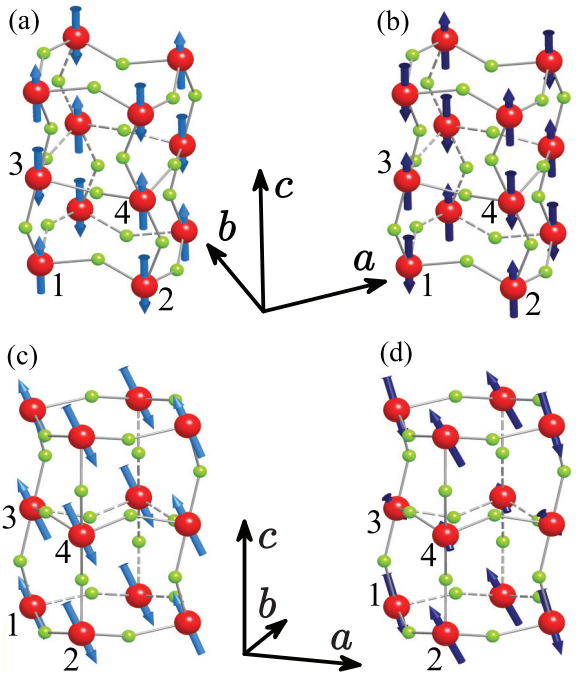

FIG. 6. (Color online) Distribution of spin [(a) and (c)] and orbital [(b) and (d)] magnetic moments as obtained in the mean-field Hartree-Fock calculations for the low-energy model of YVO_3 in the orthorhombic $Pbnm$ [(a) and (b)] and monoclinic $P2_1/a$ [(c) and (d)] phases. The vanadium atoms are indicated by the big red (dark) spheres and the oxygen atoms are indicated by the small green (grey) spheres. For the sake of clarity, the arrows for the orbital magnetic moments in the sublattice (1,2) were scaled in order to have the same length as for the spin magnetic moments. The orbital magnetic moments in the sublattice (3,4) are additionally quenched by stronger crystal field.

The type of the magnetic ground state in the orthorhombic YVO_3 is different from the one in $YTiO_3$ and $LaMnO_3$. As a result, the $\mathbf{k}$ dependence of $\boldsymbol{\mathcal{C}}(\mathbf{k})$ and $\Delta\boldsymbol{\mathcal{M}}(\mathbf{k})$ is also different. Since the net magnetic moment is parallel to the orthorhombic $\boldsymbol{a}$ axis, only $\boldsymbol{a}$ projection of $\Delta\boldsymbol{\mathcal{M}}$ is finite, while two other projections are identically equal to zero. Then, $\Delta\mathcal{M}_a(\mathbf{k})$ reaches the maximal value of $0.099\ \mu_B$ in the X point of the BZ (see Fig. 7), which exceeds the net local magnetic moment $\mathcal{M}_a^0$ by more than one order of magnitude (Table I). There are other positive contributions, originating from the X, $Z = (0,0,\frac{1}{2})$, and U points of the BZ. Nevertheless, they are well compensated by the negative contributions, coming from the T and $R = (\frac{1}{2},\frac{1}{2},\frac{1}{2})$ points of the BZ, that again results in the small value of $\Delta\mathcal{M}_a$ (Table I). This behavior is totally consistent with the form of $\mathcal{C}_a(\mathbf{k})$.

A completely different type of cancellation occurs in the monoclinic phase of YVO_3. In this case, the net orbital moment is parallel to the monoclinic $\boldsymbol{b}$ axis (Table I), and $\Delta\mathcal{M}_b(\mathbf{k})$ has the largest magnitude in the plane $k_c = \frac{1}{2}$, where the region of positive values around the point $E = (\overline{\frac{1}{2}},\frac{1}{2},\frac{1}{2})$ is nearly canceled by the region of negative values around the point $D = (\overline{\frac{1}{2}},0,\frac{1}{2})$ (see Fig. 8). This behavior is again consistent with

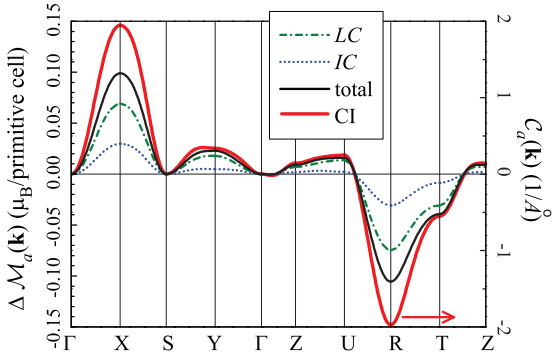

FIG. 7. (Color online) Behavior of itinerant contributions to the net orbital magnetic moment in the orthorhombic $Pbnm$ phase of YVO_3 (left axis) and corresponding Chern invariant (CI, right axis) in the reciprocal space, along high-symmetry directions of the Brillouin zone. Two partial contributions to the net orbital moment, associated with the local ($\Delta\boldsymbol{\mathcal{M}}^{LC}$) and itinerant ($\boldsymbol{\mathcal{M}}^{IC}$) circulation, are denoted as *LC* and *IC*, respectively, and the sum of these two contributions is denoted as "total".

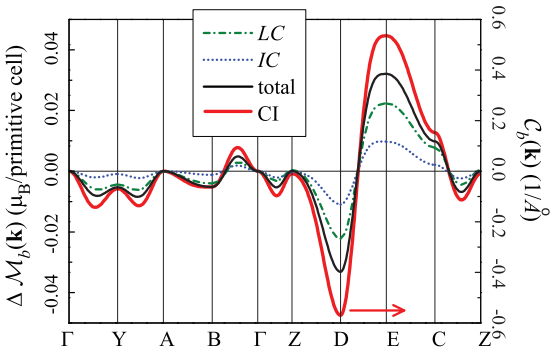

FIG. 8. (Color online) Behavior of itinerant contributions to the net orbital magnetic moment in the monoclinic $P2_1/a$ phase of YVO_3 (left axis) and corresponding Chern invariant (CI, right axis) in the reciprocal space, along high-symmetry directions of the Brillouin zone. Two partial contributions to the net orbital moment, associated with the local ($\Delta\mathcal{M}^{LC}$) and itinerant ($\mathcal{M}^{IC}$) circulation, are denoted as *LC* and *IC*, respectively, and the sum of these two contributions is denoted as "total".

the form of $\mathcal{C}_b(\mathbf{k})$ and explains the small value of integrated $\Delta\mathcal{M}_b$ in Table I.

VI. CONCLUSIONS

We have applied modern theory of the orbital magnetization to the series of distorted perovskite transition-metal oxides with a net FM moment in the ground state. Our applications cover several typical examples, including canted (but yet robust) ferromagnetism in orthorhombic $YTiO_3$ as well as the weak ferromagnetism, caused by either antisymmetric Dzyalishinskii-Moriya interactions in the orthorhombic $LaMnO_3$ and YVO_3 or imperfect cancellation of magnetization between two crystallographic sublattices in the monoclinic YVO_3. Our numerical calculations suggest that, for all considered compounds, the orbital magnetization can be well described by the "standard" expression (1), which is given by the site-diagonal part of the density matrix, while the "itinerant" corrections, suggested by the modern theory, are negligibly small. Nevertheless, the smallness of these corrections is the result of rather nontrivial cancellation of relatively large contributions coming from different parts of the BZ.

There is a big difference in the behavior of orbital magnetization and ferroelectric (FE) polarization in centrosymmetric (or nearly centrosymmetric) crystals. In the latter case, the only possibility to obtain a finite FE polarization is to break the inversion symmetry by some complex magnetic order. Such a situation is indeed realized in some multiferroic perovskite manganites, including $TbMnO_3$, $HoMnO_3$, and $YMnO_3$ [48]. Then, if the magnetic sites are located in the centers of inversion (again, as in the perovskite compounds), Eq. (8) yields $\langle\phi_{\alpha'}(\mathbf{r}-\mathbf{R})|\mathbf{r}-\mathbf{R}|\phi_\alpha(\mathbf{r}-\mathbf{R})\rangle = 0$, which means that there is no "local polarization," associated with the distribution of the electron density around these magnetic sites. Therefore, the FE polarization in this case will be totally anomalous, which can be only captured by the Berry phase of the wave functions [38,39,49]. Using similar model analysis, one can show (Ref. [39]) that this anomalous contribution in multiferroic perovskite manganites is proportional to transfer integrals between different magnetic sites and, therefore, can be regarded as an itinerant quantity, similar to $\Delta\mathcal{M}$ [50].

The behavior of the orbital magnetization in the same systems is different. In this case, there are finite local magnetic moments, which are given by the site-diagonal elements of the density matrix in the Wannier basis, and these local magnetic moments provide the main contribution to the net FM moment (if any). The itinerant corrections $\Delta\mathcal{M}$ to the FM moment, originating from the Berry phase effect, are considerably smaller. Thus the orbital magnetic moment is mainly a local quantity.

The form of $\Delta\mathcal{M}(\mathbf{k})$ in the reciprocal space follows the behavior of Chern invariants. Although the full integral over the BZ is small (or identically equals to zero in the case of Chern invariants), the integrand itself is finite and, moreover, can be strongly **k**-dependent. By tracing this discussion back to the real space by means of the Fourier transform, this would mean that the considered quantities will have nonlocal (or off-diagonal with respect to the atomic sites) contributions and, for the normal insulators studied in this work, these nonlocal contributions will be substantially larger than the local (or site-diagonal) ones. This is one of the most interesting aspects of the modern theory of the orbital magnetization, which raises new questions. Particularly, can these large nonlocal contributions be measured or can they contribute to other properties? Such a possibility was, in fact, investigated in Ref. [28], where it was argued that different (but yet gauge invariant) parts of the integrated orbital magnetization can be indeed separated experimentally by combining gyromagnetic and magneto-optical measurements, supplemented with the sum rules. Moreover, following discussions in Ref. [28], it is clear that similar strategy can be applied also for the analysis of the **k**-resolved quantities. Thus we believe that general answer to the above question should be affirmative. Nevertheless, such measurements cannot be done using conventional experimental means, because there is no such technique as "**k**-resolved magneto-optics". In this respect, one new and interesting development is the "valleytronics", which utilizes the properties of electrons, trapped in a specific region of momentum space. For example, this technique was recently proposed for the analysis of **k**-resolved optical oscillator strength and orbital magnetization of graphene [51]. Nevertheless, today this direction remains to be very specific to materials with the graphene-type electronic band structure and it is not clear whether the same type of ideas can be employed for the analysis of transition-metal oxides, including those considered in the present work.

Another interesting issue, related to the first fundamental problem outlined in the Introduction, is the direction for the improvement of SDFT. Will this large and essentially nonlocal part of itinerant magnetization contribute to the exchange-correlation energy and, in this way, improve the description of the orbital magnetization related properties? As was pointed out in Introduction, the dominant point of view so far is that the orbital magnetization is local and the main processes, which are missing in conventional DFT calculations and which are responsible for the agreement with the experimental data, can be also formulated in the local form, by considering the effect of properly screened Coulomb interactions on the

magnetic sites [8–11]. The itinerant magnetization $\Delta\boldsymbol{\mathcal{M}}(\mathbf{k})$ is not taken into account by this type of theories. However, this $\Delta\boldsymbol{\mathcal{M}}(\mathbf{k})$, being defined in terms of surface currents [17], could contribute to the exchange-correlation energy in the framework of current SDFT [6,12,18]. Then, the fact that, even in the considered transition-metal perovskite oxides, which are frequently regarded as Mott insulators, the itinerant orbital magnetization can be large in some regions of the reciprocal space, will probably revive an interest to current SDFT. However, it is still an open and largely unresolved question whether, besides an elegant general formulation (Ref. [6]), such theory can be widely used in practical calculations, which require a robust (and so far unknown) approximation for the exchange-correlation energy in terms of the current density.

ACKNOWLEDGMENTS

This work is partly supported by the grant of the Ministry of Education and Science of Russia N 14.A18.21.0889.

[1] R. M. White, *Quantum Theory of Magnetism* (Springer-Verlag, Berlin, 2007).
[2] *Magnetism and Synchrotron Radiation*, edited by E. Beaurepaire, H. Bulou, F. Scheurer, and J.-P. Kappler, Springer Proceedings in Physics Vol. 133 (Springer-Verlag, Berlin, 2010) and references therein.
[3] G. H. Lander, Phys. Scr. **44**, 33 (1991).
[4] L. L. Hirsh, Rev. Mod. Phys. **69**, 607 (1997).
[5] The relativistic SO coupling is proportional to gradient of the scalar potential [1]. Therefore, in order to produce finite SO coupling, this potential should be position-dependent (or "inhomogeneous"). The external vector potential is also position-dependent, even for the uniform magnetic field.
[6] G. Vignale and M. Rasolt, Phys. Rev. Lett. **59**, 2360 (1987); Phys. Rev. B **37**, 10685 (1988).
[7] H. J. F. Jansen, Phys. Rev. B **43**, 12025 (1991).
[8] O. Eriksson, M. S. S. Brooks, and B. Johansson, Phys. Rev. B **41**, 7311 (1990); O. Eriksson, B. Johansson, R. C. Albers, A. M. Boring, and M. S. S. Brooks, *ibid.* **42**, 2707 (1990).
[9] M. R. Norman, Phys. Rev. Lett. **64**, 1162 (1990); Phys. Rev. B **44**, 1364 (1991).
[10] I. V. Solovyev, A. I. Liechtenstein, and K. Terakura, Phys. Rev. Lett. **80**, 5758 (1998); I. V. Solovyev, *ibid.* **95**, 267205 (2005).
[11] J. Minár, J. Phys.: Condens. Matter **23**, 253201 (2011) and references therein.
[12] H. Ebert, M. Battocletti, and E. K. U. Gross, Europhys. Lett. **40**, 545 (1997).
[13] R. D. King-Smith and D. Vanderbilt, Phys. Rev. B **47**, 1651 (1993); D. Vanderbilt and R. D. King-Smith, *ibid.* **48**, 4442 (1993).
[14] R. Resta, J. Phys.: Condens. Matter **22**, 123201 (2010).
[15] D. Xiao, J. Shi, and Q. Niu, Phys. Rev. Lett. **95**, 137204 (2005).
[16] T. Thonhauser, D. Ceresoli, D. Vanderbilt, and R. Resta, Phys. Rev. Lett. **95**, 137205 (2005).
[17] D. Ceresoli, T. Thonhauser, D. Vanderbilt, and R. Resta, Phys. Rev. B **74**, 024408 (2006).
[18] J. Shi, G. Vignale, D. Xiao, and Q. Niu, Phys. Rev. Lett. **99**, 197202 (2007).
[19] T. Thonhauser, Int. J. Mod. Phys. B **25**, 1429 (2011).
[20] F. D. M. Haldane, Phys. Rev. Lett. **61**, 2015 (1988).
[21] D. Ceresoli and R. Resta, Phys. Rev. B **76**, 012405 (2007).
[22] D. Ceresoli, U. Gerstmann, A. P. Seitsonen, and F. Mauri, Phys. Rev. B **81**, 060409 (2010); M. G. Lopez, D. Vanderbilt, T. Thonhauser, and I. Souza, *ibid.* **85**, 014435 (2012).
[23] S. Coh, D. Vanderbilt, A. Malashevich, and I. Souza, Phys. Rev. B **83**, 085108 (2011).
[24] I. Dzyaloshinsky, J. Chem. Phys. Solids **4**, 241 (1958); T. Moriya, Phys. Rev. **120**, 91 (1960).
[25] D. Treves, Phys. Rev. **125**, 1843 (1962).
[26] I. V. Solovyev, J. Phys.: Condens. Matter **20**, 293201 (2008).
[27] D. J. Thouless, *Topological Quantum Numbers in Nonrelativistic Physics* (World Scientific, Singapore, 1998).
[28] I. Souza and D. Vanderbilt, Phys. Rev. B **77**, 054438 (2008).
[29] I. V. Solovyev, Phys. Rev. B **74**, 054412 (2006); J. Comput. Electron. **10**, 21 (2011).
[30] I. Solovyev, J. Phys. Soc. Jpn. **78**, 054710 (2009).
[31] O. K. Andersen, Phys. Rev. B **12**, 3060 (1975); O. Gunnarsson, O. Jepsen, and O. K. Andersen, *ibid.* **27**, 7144 (1983); O. K. Andersen, Z. Pawlowska, and O. Jepsen, *ibid.* **34**, 5253 (1986).
[32] See Supplemental Material at http://link.aps.org/supplemental/10.1103/PhysRevB.89.064428 for the details of derivation of Eqs. (9) and (10) and convergence of the orbital magnetization in the **k** space.
[33] N. Marzari and D. Vanderbilt, Phys. Rev. B **56**, 12847 (1997).
[34] I. V. Solovyev, Z. V. Pchelkina, and V. I. Anisimov, Phys. Rev. B **75**, 045110 (2007).
[35] F. Aryasetiawan, M. Imada, A. Georges, G. Kotliar, S. Biermann, and A. I. Lichtenstein, Phys. Rev. B **70**, 195104 (2004).
[36] L. Vaugier, H. Jiang, and S. Biermann, Phys. Rev. B **86**, 165105 (2012).
[37] V. I. Anisimov, J. Zaanen, and O. K. Andersen, Phys. Rev. B **44**, 943 (1991).
[38] I. V. Solovyev, Phys. Rev. B **83**, 054404 (2011); I. V. Solovyev, M. V. Valentyuk, and V. V. Mazurenko, *ibid.* **86**, 144406 (2012).
[39] I. V. Solovyev and S. A. Nikolaev, Phys. Rev. B **87**, 144424 (2013).
[40] I. V. Solovyev and Z. V. Pchelkina, Phys. Rev. B **82**, 094425 (2010); I. V. Solovyev, *ibid.* **87**, 144403 (2013).
[41] A. C. Komarek, H. Roth, M. Cwik, W.-D. Stein, J. Baier, M. Kriener, F. Bourée, T. Lorenz, and M. Braden, Phys. Rev. B **75**, 224402 (2007).
[42] In the G_a-A_b-F_c ground state, the twofold rotation around the orthorhombic $\boldsymbol{c}$ axis (combined with a translation) enters as it is, while two other rotations around the orthorhombic $\boldsymbol{a}$ and $\boldsymbol{b}$ axes enter in the combination with the time inversion. Therefore the net FM moment is allowed only along the orthorhombic $\boldsymbol{c}$ axis, while two other components are identically equal to zero.
[43] C. J. Bradley and A. P. Cracknell, *The Mathematical Theory of Symmetry in Solids* (Clarendon Press, Oxford, 1972).

[44] J. B. A. A. Elemans, B. van Laar, K. R. van der Veen, and B. O. Loopstra, J. Sol. State Chem. **3**, 238 (1971).

[45] G. Matsumoto, J. Phys. Soc. Jpn. **29**, 606 (1970).

[46] G. R. Blake, T. T. M. Palstra, Y. Ren, A. A. Nugroho, and A. A. Menovsky, Phys. Rev. B **65**, 174112 (2002).

[47] Y. Ren, T. T. M. Palstra, D. I. Khomskii, E. Pellegrin, A. A. Nugroho, A. A. Menovsky, and G. A. Sawatzky, Nature (London) **396**, 441 (1998). Note that the experimental net magnetization in the orthorhombic $Pbnm$ phase is parallel to the $\boldsymbol{a}$ axis, that is totally consistent with our finding. The experimental magnetization in the monoclinic phase is also parallel to the $\boldsymbol{a}$ direction in the *orthorhombic* setting, which corresponds to the $\boldsymbol{b}$ direction in the monoclinic $P2_1/a$ setting, again, in agreement with our finding.

[48] T. Kimura, Annu. Rev. Mater. Res. **37**, 387 (2007); S.-W. Cheong and M. Mostovoy, Nat. Mater. **6**, 13 (2007); D. Khomskii, Physics **2**, 20 (2009); Y. Tokura and S. Seki, Adv. Mater. **22**, 1554 (2010).

[49] P. Barone, K. Yamauchi, and S. Picozzi, Phys. Rev. Lett. **106**, 077201 (2011).

[50] Note that, if the transfer integrals vanish, the electronic structure will not depend on $\mathbf{k}$. Then, $\Delta\boldsymbol{\mathcal{M}}$ will also vanish, so as the anomalous polarization. Therefore both quantities can be regarded as itinerant ones, in the same sense of the word "itineracy".

[51] D. Xiao, W. Yao, and Q. Niu, Phys. Rev. Lett. **99**, 236809 (2007); W. Yao, D. Xiao, and Q. Niu, Phys. Rev. B **77**, 235406 (2008).